J|A|C|S
ARTICLES
Published on Web 07/12/2006

Propene Activation by the Oxo-Iron Active Species of Taurine/ α-Ketoglutarate Dioxygenase (TauD) Enzyme. How Does the Catalysis Compare to Heme-Enzymes?

Sam P. de Visser*

Contribution from the Manchester Interdisciplinary Biocenter and the School of Chemical Engineering and Analytical Science, The University of Manchester, Sackville Street, P.O. Box 88, Manchester M60 1QD, United Kingdom

Received March 7, 2006; E-mail: sam.devisser@manchester.ac.uk

Abstract: Density functional calculations on the oxygenation reaction of propene by a model for taurine/ α-ketoglutarate dioxygenase (TauD) enzyme are presented. The oxo-iron active species of TauD is shown to be a powerful and aggressive oxidant, which is able to hydroxylate C−H bonds and epoxidize C═C bonds with low barriers. In the case of propene oxygenation, the hydroxylation and epoxidation mechanisms are competitive on a dominant quintet spin state surface. We have compared the mechanism and thermodynamics of TauD with oxo-iron heme catalysts, such as the cytochromes P450, and found some critical differences. The TauD model is found to be much more reactive toward oxygenation of substrates than oxo-iron complexes in a heme environment with much lower reaction barriers. We have analyzed this and assigned this to the strength of the O−H bond formed after hydrogen abstraction from a substrate, which is at least 10 kcal mol^{-1} stronger in five-coordinated oxo-iron nonheme complexes than in six-coordinated oxo-iron heme complexes. Since, the metal in TauD enzymes is five-coordinated, whereas in heme-enzymes it is six-coordinated there are some critical differences in the valence molecular orbitals. Thus, in oxo-iron heme catalysts one of the antibonding π^* orbitals is replaced by a low-lying nonbonding δ orbital resulting in a lower overall spin state. Moreover, heme-enzymes have an extra oxidation equivalent located on the heme, which is missing in non-heme oxo-iron catalysts. As a result, the oxo-iron species of TauD reacts via single-state reactivity on a dominant quintet spin state surface, whereas oxo-iron heme catalysts react via two-state reactivity on competing doublet and quartet spin states.

Introduction

Monoxygenase enzymes, such as the cytochromes P450 (P450), catalyze vital processes in biosystems like detoxification reactions and are also involved in drug metabolism and the biosynthesis of hormones.[1] This catalytic versatility arises since the enzymes are able to catalyze C−H hydroxylations, C═C epoxidations as well as sulfoxidations.[2] The active form of P450 enzymes (Compound I, CpdI) is the oxo-iron species, which is embedded in a heme-group and bound via a thiolate linkage of a cysteinate residue to the protein backbone.[3] The cysteinate residue was found to incur a push-effect on the oxo-iron group, thereby enabling the system with oxidative properties.[4] By contrast, in other heme-enzymes such as horseradish peroxidase (HRP) or cytochrome *c* peroxidase (C*c*P) the metal is linked to the peptide backbone via an imidazole linkage of a histidine residue.[5] Since histidine is a weak ligand, it influences the electronic properties of the catalyst and hence HRP and C*c*P do not work as monoxygenases but rather as peroxidases.

Other enzymes with a central oxo-iron active species are the α-ketoglutarate dioxygenase (αKGD) class of enzymes, which are also able to hydroxylate C−H bonds and epoxidize C═C bonds of substrates.[6] The big difference between αKGD and P450 enzymes, however, is the fact that the dioxygenases are non-heme enzymes that do not contain a co-enzyme but utilize α-ketoglutarate as a cofactor instead. Thus, αKGD binds molecular oxygen of which one atom is used to convert α-ketoglutarate into succinate and carbon dioxide thereby creating an oxo-iron active species. By contrast, in P450 enzymes after molecular oxygen binding a reduction followed by two protonation steps leads to water and the oxo-iron active species.[7] As a consequence, the heme-enzymes have amino acid residues and bound water molecules that shuttle protons into

(1) Ortiz de Montellano, P. R., Ed. *Cytochrome P450: Structure, Mechanism and Biochemistry*, 3rd ed.; Kluwer Academic/Plenum Publishers: New York, 2004.
(2) (a) Sono, M.; Roach, M. P.; Coulter, E. D.; Dawson, J. H. *Chem. Rev.* **1996**, *96*, 2841−2887. (b) Woggon, W.-D. *Top. Curr. Chem.* **1996**, *184*, 39−96. (c) Groves, J. T. *Proc. Natl. Acad. Sci. U.S.A.* **2003**, *100*, 3569−3574. (d) Groves, J. T. Chapter 1 in ref 1, pp 1−43.
(3) (a) Schlichting, I.; Berendzen, J.; Chu, K.; Stock, A. M.; Maves, S. A.; Benson, D. E.; Sweet, R. M.; Ringe, D.; Petsko, G. A.; Sligar, S. G. *Science* **2000**, *287*, 1615−1622. (b) Loew, G. H.; Harris, D. L. *Chem. Rev.* **2000**, *100*, 407−419. (c) Harris, D. L. *Curr. Opin. Chem. Biol.* **2001**, *5*, 724−735. (d) Meunier, B.; de Visser, S. P.; Shaik, S. *Chem. Rev.* **2004**, *104*, 3947−3980.
(4) (a) Dawson, J. H.; Holm, R. H.; Trudell, J. R.; Barth, G.; Linder, R. E.; Bunnenberg, E.; Djerassi, C.; Tang, S. C. *J. Am. Chem. Soc.* **1976**, *98*, 3707−3709. (b) Poulos, T. L. *J. Biol. Inorg. Chem.* **1996**, *1*, 356−359.
(5) (a) Berglund, G. I.; Carlsson, G. H.; Smith, A. T.; Szöke, H.; Henriksen, A.; Hajdu, J. *Nature (London)* **2002**, *417*, 463−468. (b) Goodin, D. B.; McRee, D. E. *Biochemistry* **1993**, *32*, 3313−3324.
(6) (a) Bugg, T. D. H. *Tetrahedron* **2003**, *59*, 7075−7101. (b) Costas, M.; Mehn, M. P.; Jensen, M. P.; Que Jr., L. *Chem. Rev.* **2004**, *104*, 939−986.

Scheme 1. Conversion of the Resting State of TauD into Its Active Form (oxo-iron complex)

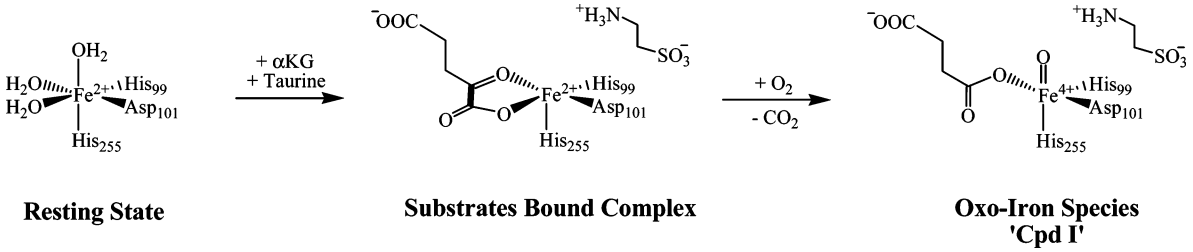

Resting State **Substrates Bound Complex** **Oxo-Iron Species 'Cpd I'**

the active site, while this is not the case in αKGD enzymes so that the local environment of the active center of the catalyst is very different. Nevertheless, in both enzymes (αKGD and P450) the active species is the oxo-iron species that is able to catalyze C−H hydroxylations and C═C epoxidations. In this paper, we will make a direct comparison between the two enzyme classes and study the fundamental differences in catalytic properties of the two enzyme active sites using a model reaction.

α-Ketoglutarate dioxygenase (αKGD) is a large class of enzymes involved in many important biochemical processes in bacteria as well as in mammals and humans.[6] As such, they are involved in the biosynthesis of collagen in mammals, antibiotics in bacteria and detoxification processes in various biosystems.[6,8] In addition, it was found that DNA base repair is catalyzed by αKGD enzymes, whereby the methylated DNA base is hydroxylated and subsequently due to formaldehyde release converted into the original base.[9] One of the best studied αKGD enzymes is taurine/αKGD (TauD), which hydroxylates taurine into amino acetaldehyde and sulfite.[10−12] Scheme 1 shows the basic reaction mechanism of the conversion of the resting state of TauD into the oxo-iron species. In TauD, the central iron atom is bound to the peptide environment via linkages with the side chains of two histidine (His_{99}, His_{255}) and an aspartic acid (Asp_{101}) group. In the resting state (Scheme 1) three water molecules occupy the remaining three ligand sites of the iron, but upon binding of the two substrates, i.e., α-ketoglutarate (αKG) and taurine, the three water molecules are displaced.[13−15] Note that taurine does not bind directly to the iron complex but somewhere in the vicinity, while αKG binds as a bidentate ligand. The substrates bound complex (Scheme 1) has been characterized by X-ray and Mössbauer spectroscopy, and the studies indeed confirmed that the iron changes from six-coordination to five-coordination after both substrates bind.[13−15] Subsequently, dioxygen binding to the active site leads to conversion of αKG to succinate and carbon dioxide while an oxo-iron species is formed. This is the rate-determining step in the catalytic cycle and occurs so fast that information beyond this point is limited.[16] However, two intermediates have been identified after the dioxygen binding steps, although their lifetime was short.[15] Isotope effect studies of taurine vs taurine-d_2 characterized the first intermediate as the one responsible for the hydrogen abstraction step and is therefore presumably the oxo-iron species.[17] Further evidence of the oxo-iron species was obtained from isotopic substitution studies whereby $^{18}O_2$ was added to the enzyme. This resulted in a downshift of the Fe−O vibration analogously to other oxo-iron systems, but different from iron-peroxide complexes.[18] Therefore, in contrast to P450 where the oxo-iron complex is elusive and has never been detected experimentally, in TauD it was trapped and characterized. The second intermediate identified after dioxygen binding was assigned as a product complex.[19] Other studies showed that in the absence of substrate a self-hydroxylation reaction occurs of the Tyr_{73} amino acid.[20] This amino acid is located close to the oxo-iron group and normally functions as substrate binding group.

Thus, heme and non-heme enzymes both are able to create an oxo-iron active center and catalyze oxygenation reactions. However, the active species of αKGD and P450 enzymes have strong geometric differences, namely in P450 Cpd I is six-coordinated, whereas in αKGD the active species is five-coordinated. As a result, the two active species will have differences in molecular orbitals which may result in reactivity differences.[21,22] To address these issues, we have performed detailed density functional theoretic calculations on models of the active species of P450, HRP, and αKGD and studied their reactivity toward a typical substrate, i.e., propene. Earlier studies[23,24] identified the reactivity differences between HRP

(7) (a) Makris, T. M.; Denisov, I.; Schlichting, I.; Sligar, S. G. Chapter 5 in ref 1, pp 149−181. (b) Kumar, D.; Hirao, H.; de Visser, S. P.; Zheng, J.; Wang, D.; Thiel, W.; Shaik, S. *J. Phys. Chem. B* **2005**, *109*, 19946−19951. (c) Shaik, S.; Kumar, D.; de Visser, S. P.; Altun, A.; Thiel, W. *Chem. Rev.* **2005**, *105*, 2279−2328.
(8) See, e.g., (a) Choroba, O. W.; Williams, D. H.; Spencer, J. B. *J. Am. Chem. Soc.* **2000**, *122*, 5389−5390. (b) Higgins, L. J.; Yan, F.; Liu, P.; Liu, H.-W.; Drennan, C. L. *Nature (London)* **2005**, *437*, 838−844.
(9) See, for instance: (a) Trewick, S. C.; Henshaw, T. F.; Hausinger, R. P.; Lindahl, T.; Sedgwick, B. *Nature (London)* **2002**, *419*, 174−178. (b) Falnes, P. Ø.; Johansen, R. F.; Seeberg, E. *Nature (London)* **2002**, *419*, 178−182. (c) Duncan, T.; Trewick, S. C.; Koivisto, P.; Bates, P. A.; Lindahl, T.; Sedgwick, B. *Proc. Natl. Acad. Sci., USA* **2002**, *99*, 16660−16665. (d) Aas, P. A.; Otterlei, M.; Falnes, P. Ø.; Vågbø, C. B.; Skorpen, F.; Akbari, M.; Sundheim, O.; Bjørås, M.; Slupphaug, G.; Seeberg, E.; Krokan, H. E. *Nature (London)* **2003**, *421*, 859−863. (e) Mishina, Y.; Duguid, E. M.; He, C. *Chem. Rev.* **2006**, *106*, 215−232.
(10) Solomon, E. I.; Brunold, T. C.; Davis, M. I.; Kemsley, J. N.; Lee, S.-K.; Lehnert, N.; Neese, F.; Skulan, A. J.; Yang, Y.-S.; Zhou, J. *Chem. Rev.* **2000**, *100*, 235−349.
(11) Ryle, M. J. Hausinger, R. P. *Curr. Opin. Chem. Biol.* **2002**, *6*, 193−201.
(12) Bollinger Jr., J. M.; Price, J. C.; Hoffart, L. M.; Barr, E. W.; Krebs, C. *Eur. J. Inorg. Chem.* **2005**, 4245−4254.
(13) Elkins, J. M.; Ryle, M. J.; Clifton, I. J.; Dunning Hotopp, J. C.; Lloyd, J. S.; Burzlaff, N. I.; Baldwin, J. E.; Hausinger, R. P.; Roach, P. L. *Biochemistry* **2002**, *41*, 5185−5192.
(14) O'Brien, J. R.; Schuller, D. J.; Yang, V. S.; Dillard, B. D.; Lanzilotta, W. N. *Biochemistry* **2003**, *42*, 5547−5554.
(15) Price, J. C.; Barr, E. W.; Tirupati, B.; Bollinger Jr., J. M.; Krebs, C. *Biochemistry* **2003**, *42*, 7497−7508.
(16) Grzyska, P. K.; Ryle, M. J.; Monterosso, G. R.; Liu, J.; Ballou, D. P.; Hausinger, R. P. *Biochemistry* **2005**, *44*, 3845−3855.
(17) Krebs, C.; Price, J. C.; Baldwin, J.; Saleh, L.; Green, M. T.; Bollinger Jr., J. M. *Inorg. Chem.* **2005**, *44*, 742−757.
(18) Proshlyakov, D. A.; Henshaw, T. F.; Monterosso, G. R.; Ryle, M. J.; Hausinger, R. P. *J. Am. Chem. Soc.* **2004**, *126*, 1022−1023.
(19) Price, J. C.; Barr, E. W.; Hoffart, L. M.; Krebs, C.; Bollinger Jr., J. M. *Biochemistry* **2005**, *44*, 8138−8147.
(20) (a) Ryle, M. J.; Koehntop, K. D.; Liu, A.; Que Jr., L.; Hausinger, R. P. *Proc. Natl. Acad. Sci., U.S.A.* **2003**, *100*, 3790−3795. (b) Koehntop, K. D.; Marimanikkupam, S.; Ryle, M. J.; Hausinger, R. P.; Que Jr., L. *J. Biol. Inorg. Chem.* **2006**, *11*, 63−72.
(21) (a) Decker, A.; Solomon, E. I. *Angew. Chem., Int. Ed.* **2005**, *44*, 2252−2255. (b) Kumar, D.; Hirao, H.; Que Jr., L.; Shaik, S. *J. Am. Chem. Soc.* **2005**, *127*, 8026−8027.
(22) de Visser, S. P. *Angew. Chem., Int. Ed.* **2006**, *45*, 1790−1793.
(23) (a) de Visser, S. P.; Ogliaro, F.; Sharma, P. K.; Shaik, S. *Angew. Chem., Int. Ed.* **2002**, *41*, 1947−1951. (b) de Visser, S. P.; Ogliaro, F.; Sharma, P. K.; Shaik, S. *J. Am. Chem. Soc.* **2002**, *124*, 11809−11826.

and P450 and assigned these due to the axial ligand that entices either a push or pull-effect on the oxo-iron group. Specifically, in HRP the reaction barriers were lower and during the reaction process the metal was kept in lower oxidation states (Fe^{III}). Moreover, HRP reacted via dominant epoxidation, whereas P450 showed dominant hydroxylation of the methyl group of propene. The calculations showed that generally C−H hydroxylation and C═C epoxidation mechanisms are close in energy and subtle external interactions, such as hydrogen bonding or an applied external electric field, were found to be sufficient to change the regioselectivity of the reaction from dominant epoxidation in the gas-phase to C−H hydroxylation in a dielectric constant of $\epsilon = 5.7$.[23,25] The question is how the oxo-iron complex in αKGD compares to the reactivity patterns of P450 and HRP. To test this, we ran DFT calculations on a TauD model complex and tested its reactivity vis-à-vis propene and compared the reaction mechanisms, thermodynamics, electronic changes, and kinetic isotope effects with earlier work on P450 and HRP catalysts. Although propene is not the natural substrate of TauD it will give us the opportunity to compare the properties of the TauD active site with oxo-iron heme-enzymes directly. As will be shown here, αKGD is a very aggressive oxidant which can catalyze monoxygenation processes with much lower barriers than corresponding heme-enzymes.

Methods

All calculations were performed using commonly accepted procedures, which we will summarize for completeness here.[22,26] We use a model of the active site of TauD as based upon the 1OS7 pdb of O'Brien et al.[14] The model contains the side chains of His_{99}, Asp_{101}, and His_{255}, which were abbreviated with imidazole and acetate. Green[27] showed that imidazole is a better mimic of a histidine bound to iron than imidazolate, therefore we also used imidazole groups for the histidine ligands here. Taurine was replaced by propene, so that we can compare the reaction mechanism and thermodynamics of the model with earlier work on oxo-iron porphyrin models of P450 and HRP enzymes.[23−25] During the process of generating the oxo-iron species, α-ketoglutarate is converted into succinate and carbon dioxide. We abbreviated succinate by acetate and kept CO_2 in the model, although it was inactive. To improve the visibility of the structures, in some figures we manually removed the CO_2 molecule from the optimized geometries. We added the oxo group and hydrogen atoms to the Cartesian coordinates of the 1OS7 pdb manually, to get a model with stoichiometry $[FeC_{14}H_{20}N_4O_7]^0$. The complete reaction profile for epoxidation and hydroxylation were studied on each of the possible spin state surfaces (triplet, quintet, and septet spin states), which are identified by a superscript next to the label of each structure. We also calculated the oxo-iron species in the singlet spin state, but found it much higher in energy than the quintet spin state (by 20 kcal mol^{-1}), therefore we did not pursue this spin surface further.

All calculations utilize the UB3LYP hybrid density functional method with a double-ζ quality basis set (LACVP) on iron and a 6-31G basis set on the rest of the atoms.[28,29] All structures were fully optimized (without constraints) in Jaguar 5.5.[30,31] Since, Jaguar does not have the possibility of calculating the vibrational frequencies analytically, we calculated these in Gaussian-98 to save CPU time.[32] Previous studies of ours showed that frequencies calculated in Jaguar and Gaussian-98 give similar results.[23b,33] The transition states described here had one imaginary frequency for the correct mode, whereas all local minima had real frequencies only. The complete project resulted in a large set of data including spin densities, charges as well as detailed geometry scans which are all relegated to the supplementary information while we will only focus on the major trends here.

The effect of the environment was tested with the self-consistent reaction field (SCRF) model as implemented in Jaguar with dielectric constants $\epsilon = 5.7$ and $\epsilon = 10.65$.

The kinetic isotope effect (KIE) of replacing hydrogen by deuterium atoms in the substrate was estimated using two different models.[23b] The Eyring Model (KIE_E) is the semiclassical KIE and is estimated from the free energies of activation ($\Delta G^{\ddagger}_H$) of the deuterium substituted and reference systems, with R being the gas constant and T the estimated temperature (298.15 K).

$$KIE_E = k_H/k_D = \exp\{(\Delta G^{\ddagger}_D - \Delta G^{\ddagger}_H)/RT\} \qquad (1)$$

Subsequent incorporation of the tunneling correction due to Wigner gives the KIE_W as a product of the Eyring KIE_E with the tunneling ratio (Q_{tH}/Q_{tD}) as follows:

$$KIE_W = KIE_E * Q_{tH}/Q_{tD} \qquad (2)$$

$$Q_t = 1 + \frac{1}{24}\left(\frac{h\nu}{kT}\right)^2 \qquad (3)$$

In this equation, k is Boltzmann's constant, h is Planck's constant, and ν is the magnitude of the imaginary frequency in the transition state. Kinetic isotope effects were calculated using the data from the Gaussian frequency calculations.

Results

Molecular Orbitals of the Oxo-Iron Species of αKGD. Transition metal complexes generally contain many close-lying electronic (and spin) states and therefore we will start with summarizing the important molecular orbitals in the reaction process. Figure 1 shows the high-lying occupied and low-lying virtual orbitals of the oxo-iron complex of αKGD, which we analogously to oxo-iron heme-enzymes will designate Com-

(24) Kumar, D.; de Visser, S. P.; Sharma, P. K.; Derat, E.; Shaik, S. *J. Biol. Inorg. Chem.* **2005**, *10*, 181−189.
(25) Shaik, S.; de Visser, S. P.; Kumar, D. *J. Am. Chem. Soc.* **2004**, *126*, 11746−11749.
(26) de Visser, S. P. *J. Phys. Chem. A* **2005**, *109*, 11050−11057.
(27) Green, M. T. *J. Am. Chem. Soc.* **2000**, *122*, 9495−9499.
(28) (a) Becke, A. D. *J. Chem. Phys.* **1993**, *98*, 5648−5652. (b) Lee, C.; Yang, W.; Parr, R. G. *Phys. Rev. B* **1988**, *37*, 785−789.
(29) Hay, J. P.; Wadt, W. R. *J. Chem. Phys.* **1985**, *82*, 270−283.
(30) Jaguar 5.5; Schrödinger, Inc.: Portland OR, 2000.
(31) Initially, we attempted to calculate the reaction profile with one atom of each ligand bound to iron fixed in position so that the structure matches the 1OS7 pdb. However, this created technical problems with frequency calculations with several imaginary modes. Therefore, we subsequently removed all constraints from the geometries and did full geometry optimizations in Jaguar 5.5. Previous theoretical studies ((a) Siegbahn, P. E. M. *Q. Rev. Biophys.* **2003**, *36*, 91−145. (b) Kumar, D.; Hirao, H.; de Visser, S. P.; Zheng, J.; Wang, D.; Thiel, W.; Shaik, S. *J. Phys. Chem. B* **2005**, *109*, 19946−19951) on enzyme models showed differences of less than 2 kcal mol^{-1} between the fully optimized structure and a constraint one.
(32) Frisch, M. J. et al., Gaussian-98, Gaussian, Inc., full reference see Supporting Information.
(33) Ogliaro, F.; Harris, N.; Cohen, S.; Filatov, M.; de Visser, S. P.; Shaik, S. *J. Am. Chem. Soc.* **2000**, *122*, 8977−8989.

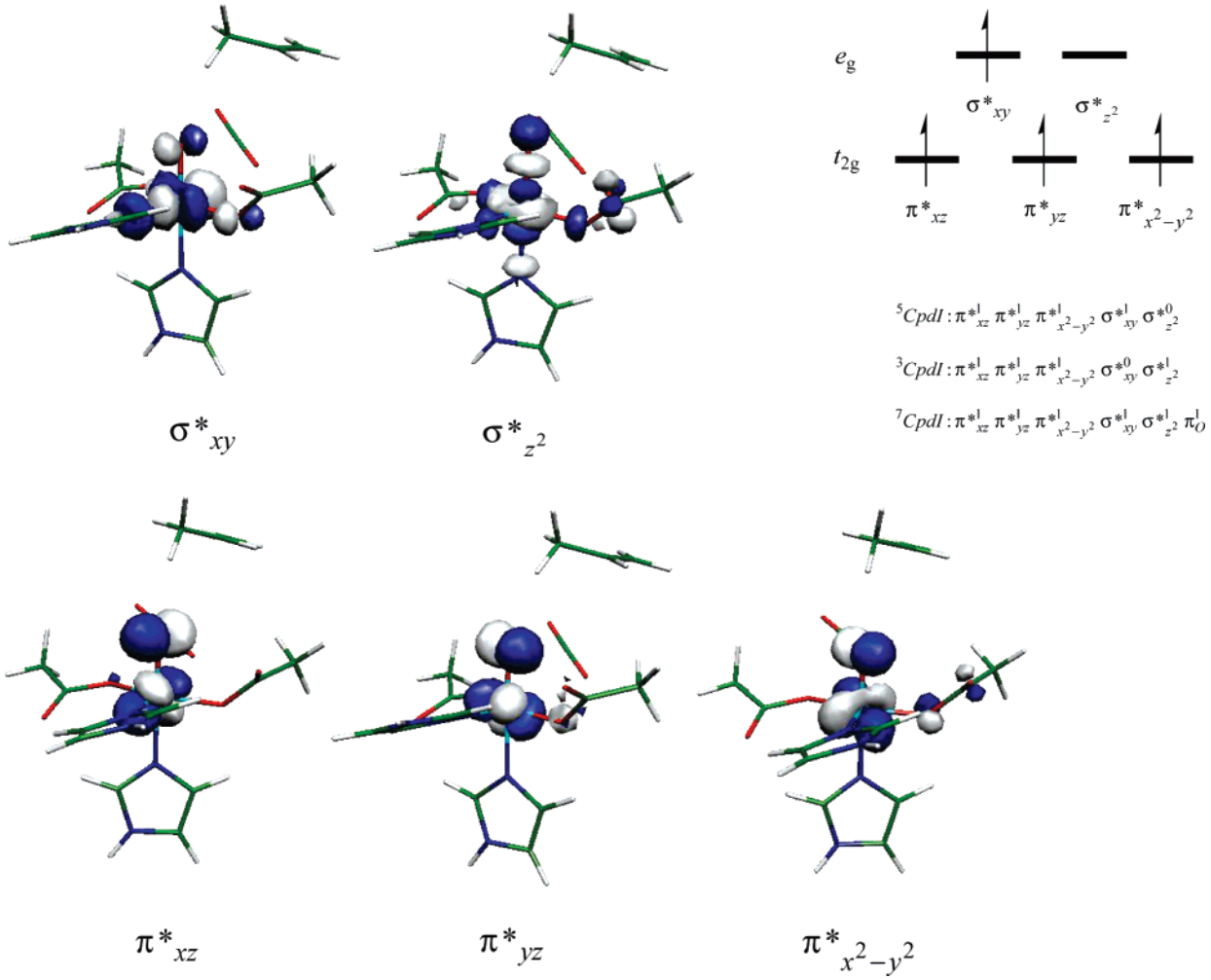

Figure 1. High-lying occupied and low-lying virtual orbitals of αKGD Cpd I and the occupation of these orbitals in the triplet, quintet and septet spin states.

pound I (Cpd I). The five orbitals depicted in Figure 1 all originate from the metal 3d orbitals and split in the typical 3-below-2 ($t_{2g}-e_g$) set of orbitals. We label the individual orbitals analogously to the ones obtained for oxo-iron complexes in heme-environments, such as P450 or HRP, for easier comparison.[7c] Thus, the three t_{2g} orbitals are π^* type and are dominated by the antibonding interactions of a metal 3d-orbital with a 2p-orbital on the oxo-group. By contrast, the e_g set of orbitals are σ^*-type orbitals for the antibonding interactions along the *z*-axis ($His_{255}-Fe-O$) and for the interactions in the *xy*-plane, whereby the metal interacts with the His_{99}, Asp_{101} and succinate ($Succ^-$) ligands. In the quintet spin state, which we find as the ground state, the orbital occupation is: $\pi^*_{xz}{}^1\pi^*_{yz}{}^1\pi^{*1}_{x^2-y^2}\sigma^*_{xy}{}^1\sigma^{*0}_{z^2}$. Mössbauer spectra and earlier DFT calculations indeed confirm the quintet spin state as the ground state of αKGD Cpd I.[15,17,34] Siegbahn et al.[34] calculated the dioxygen activation in clavaminic acid synthase, which belongs to the group of αKGD enzymes and found the quintet state well separated from the septet (by 12.6 kcal mol^{-1}) and the triplet (by 18.1 kcal mol^{-1}) spin states. We find energy differences of 7.2 and 15.8 kcal mol^{-1}, respectively, between the quintet ground state and the lowest lying septet and triplet spin states, which is in reasonable agreement with the results of ref 34. The differences between this work and ref 34 are the result of differences in the model, namely for the calculation of the energy differences Siegbahn et al.[34] abbreviated the imidazole groups by ammonia molecules and the carboxylic acid groups by formate, while we use a larger model. Nevertheless, the spin state ordering is the same and quantitative similar results are obtained as the model described here. In phenylalanine hydroxylase (PAH), which is also a non-heme oxo-iron complex but with a six-coordination sphere, Shiota and Yoshizawa[35] also obtained a quintet ground state, and found it well separated from the triplet and septet spin states, so that this seems to be a common feature among non-heme oxo-iron enzymes. In the septet spin state, we find the complete metal d-block singly occupied as well as a lone pair orbital on the oxo group (π_O).

The optimized geometries of αKGD Cpd I in the quintet, triplet and septet spin states are depicted in Figure 2. In the quintet spin state Cpd I has an Fe−O distance of 1.653 Å, which is typical for oxo-iron complexes and matches well with the experimentally obtained distance for Cpd I of HRP (1.7 Å) and catalase (1.76 Å).[5a,36] Theoretical models of Cpd I of HRP and P450 predicted Fe−O distances of 1.621 and 1.651 Å,[37]

(34) (a) Bassan, A.; Borowski, T.; Siegbahn, P. E. M. *Dalton Trans.* **2004**, 3153−3162. (b) Borowski, T.; Bassan, A.; Siegbahn, P. E. M. *Chem.—Eur. J.* **2004**, *10*, 1031−1041.

(35) Shiota, Y.; Yoshizawa, K. *J. Phys. Chem. B* **2004**, *108*, 17226−17237.

(36) Andreoletti, P.; Pernoud, A.; Sainz, G.; Gouet, P.; Jouve, H. M. *Acta Cryst. D* **2003**, *59*, 2163-2168.

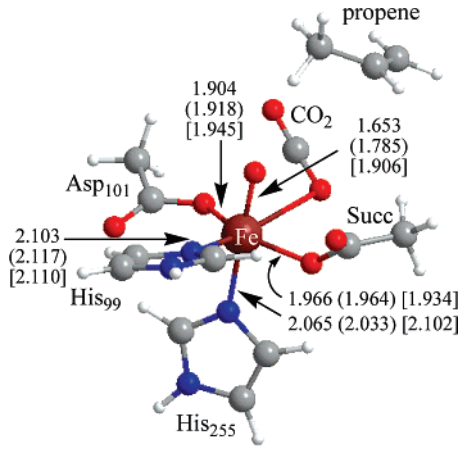

^{5}**1** (^{3}**1**) [^{7}**1**]

Figure 2. Optimized geometries of Cpd I of αKGD (^{5,3,7}**1**) with bond lengths in Å. Amino acid residues are labeled according to the 1OS7 pdb.

respectively, which are values very close to the ones obtained here for ^{5}Cpd I. The Fe−O distance in the triplet spin state is significantly enhanced with respect to the quintet spin state due to single occupation of the antibonding $\sigma^*_{z^2}$ orbital for the interaction of N_{His255}−Fe−O in ^{3}Cpd I, whereas this orbital is empty in ^{5}Cpd I. In the septet spin state, the Fe−O distance grows to 1.906 Å due to even more antibonding character of the Fe−O bond. The Fe−N distances in Cpd I of αKGD are between 2.03 and 2.12 Å, whereas this distance in HRP Cpd I was 2.1 Å.[37] Therefore, replacing the heme ligand by histidine and aspartic acid groups does not change the Fe−N distance considerably. This is mainly since the histidine residues are weak ligands with limited bonding interactions, especially with the metal 3d-orbitals. As a result, the histidine ligands contain little spin density in any of the spin states. There is no crystal structure available of the oxo-iron complex of TauD, only of the substrate bound complex.[14] In the substrate bound complex, the carboxylic acid groups of αKG and Asp_{101} are at an average distance of 2.02 Å,[14] which is in excellent agreement with our calculated values of 1.904 and 1.966 Å (Figure 2). The experimental Fe−N_{His} distances, however, are somewhat larger than obtained here (2.5 Å).[14] Nevertheless, since the histidine ligands are neutral and their electronic interactions with the metal are limited, we do not expect this to have serious consequences on the reaction energetics.

Propene Epoxidation by the Oxo-Iron Species of αKGD. Subsequently, we investigated the epoxidation mechanism of propene by αKGD Cpd I (^{3,5,7}**1**), Figure 3. The reaction proceeds via an initial C−O bond activation (via barrier **TS1**) to form a radical intermediate (**2**), which via a ring-closure barrier (**TS2**) leads to epoxide products (**3**). In the quintet spin state, the C−O bond activation step is accomplished with a simultaneous electron transfer from the substrate into the vacant $\sigma^*_{z^2}$ orbital to produce a radical intermediate ^{5}**2** with orbital occupation: $\pi^*_{xz}{}^1\pi^*_{yz}{}^1\pi^*_{x^2-y^2}\sigma^*_{xy}{}^1\sigma^{*1}_{z^2}\varphi_{CH}{}^1$, whereby the φ_{CH} orbital is the radical located on the central carbon atom of propene. Thus, on the quintet spin state surface the system gains radical character with six singly occupied orbitals including the complete 3d-metal block, while in the reactant only four molecular orbitals are singly occupied. This extra exchange stabilization lowers not only the energy of the intermediate complex considerably, but also of the transition state (^{5}**TS1**) to only 4.8 kcal mol^{-1}. The initial C=C bond activation is the rate-determining step leading to an intermediate, which is well lower in energy than the reactants (by 15.8 kcal mol^{-1}) and is separated by a small ring-closure barrier leading to products (of 2.6 kcal mol^{-1}). Therefore, the intermediate will have a limited lifetime during which rearrangements can occur. Note that the C−O bond activation results in a shift of the carboxylic acid group of Asp_{101}, which changes from a monodentate ligand in Cpd I to a bidentate ligand in ^{5}**2**, whereas in the product complex it transfers back to a monodentate ligand. We did not observe this in the triplet and septet spin states where the carboxylic acid group stayed virtually in the same position along the complete reaction pathway. No noticeable geometric changes were observed for the other ligands. In the septet spin state, the His_{255} was located in the *xy*-plane of symmetry so that the ligand position trans to the substrate was empty. The triplet spin mechanism is essentially similar to the one obtained for the quintet spin state but is well higher in energy and will play a limited role of importance.

In the septet spin state, an intermediate is reached with the same orbital occupation as in the quintet spin state, hence the two surfaces approach each other closely (vide infra). As a result the geometries of ^{5}**2** and ^{7}**2** are very similar. Nevertheless, the septet spin surface via ^{7}**TS1** is significantly higher lying than the pathway via ^{5}**TS1**, and it is expected that the occupation of the septet spin state will be limited. Because of the lack of available low-lying virtual orbitals in the septet spin state needed for absorption of one extra electron the epoxidation mechanism encounters a huge barrier from intermediate to products. As a consequence of the missing second oxidation equivalent in the septet spin state, instead of generating epoxide products the substrate dissociates into formaldehyde and $CH_3CH\bullet\bullet$ (^{7}**3′** products).

Propene Hydroxylation by the Oxo-Iron Species of αKGD. Figure 4 shows the potential energy profiles of the reaction of ^{5,3,7}**1** with propene leading to propenol products. The reaction follows the typical Groves mechanism of hydroxylation[38] with an initial hydrogen abstraction (via barrier **TS3**) to form a hydroxo-iron with a nearby allene radical (**4**) followed by a radical rebound (via barrier **TS4**) to form propenol products (**5**). The lowest hydrogen abstraction barrier is via ^{5}**TS3** and is only 5.4 kcal mol^{-1}, which is just 0.6 kcal mol^{-1} higher than the lowest epoxidation barrier. Similar to the epoxidation mechanism in the septet and quintet spin states a radical intermediate with $\pi^*_{xz}{}^1\pi^*_{yz}{}^1\pi^{*1}_{x^2-y^2}\sigma^*_{xy}{}^1\sigma^{*1}_{z^2}\varphi_{allene}{}^1$ occupation is created (^{5,7}**4**), whereby the latter orbital is the radical located on the allene group (φ_{allene}). Since, ^{5}**4** and ^{7}**4** have the same orbital occupation they are virtually degenerate and within 1 kcal mol^{-1} of each other (vide infra). The process from ^{5}**4** to ^{5}**5** encounters a small rebound barrier of 3.5 kcal mol^{-1}, and therefore the radical intermediate will have sufficient lifetime to undergo rearrangement.

Again, due to the missing oxidation equivalent on the septet spin surface the process from intermediates to products leads to an excited state with a biradical on the propenol product. Geometrically this structure has a twisted terminal CH_2 group

(37) de Visser, S. P.; Shaik, S.; Sharma, P. K.; Kumar, D.; Thiel, W. *J. Am. Chem. Soc.* **2003**, *125*, 15779−15788.

(38) Groves, J. T.; McClusky, G. A. *J. Am. Chem. Soc.* **1976**, *98*, 859−861.

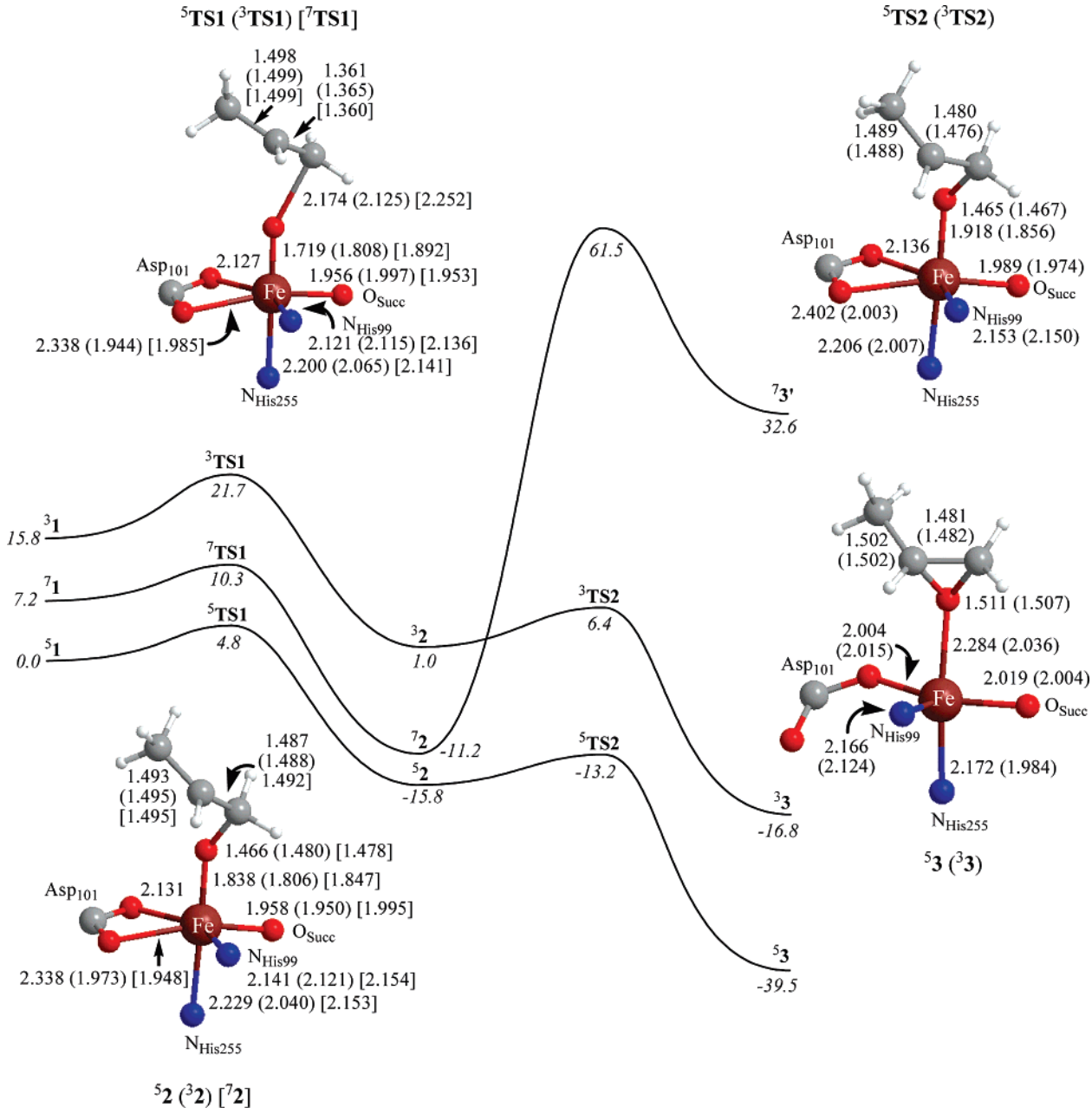

Figure 3. Reaction profile of the epoxidation of propene by ^{3,5,7}**1** (αKGD) as obtained from UB3LYP/LACVP optimizations in Jaguar. All energies (in kcal mol^{-1}) are at the LACV3P+* level of theory with ZPE corrections included. Also shown are extracts of the optimized geometries along the pathway with bond lengths in Å.

that is perpendicular to the CH group of propenol, with a typically long C−C bond of 1.459 Å, while in the triplet and quintet spin states this bond is only 1.338 Å as is normally the case for a C═C double bond.

External Effects that Influence the Relative Barriers. Subsequently, we tested the effect of a dielectric constant on the relative energies of the rate-determining steps (**TS1**, **TS3**) of the epoxidation and hydroxylation reaction processes. Although, only minor changes were obtained, in a dielectric constant of $\epsilon = 5.7$ or $\epsilon = 10.65$ the epoxidation barrier is destabilized. As a result, the hydroxylation barrier is the lowest lying in $\epsilon = 10.65$: ΔE+ZPE is 5.4 (^{5}**TS3**) vs 5.7 (^{5}**TS1**) kcal mol^{-1}. The same happens in the triplet and septet spin states, but these barriers stay well higher than the quintet spin pathway. Thus, similarly to P450 and HRP systems also in αKGD models the hydroxylation barriers are stabilized in systems with a dielectric constant of $\epsilon = 5.7$ or $\epsilon = 10.65$ although by a much lesser amount. In particular, in a dielectric constant competitive hydroxylation and epoxidation mechanisms may be expected.

To find out whether hydrogen bonding interactions as appear in the enzyme pocket influence the reaction barriers, we added two hydrogen bonded water molecules to the protons of the N−H groups of the imidazole ligands at a distance of 2.5 Å. In the crystal structure, these water molecules appear at a somewhat further distance of 2.946 and 3.618 Å,[14] but this will give a clear indication on the possible effects of hydrogen bonding on the relative energies of the barriers. At the LACVP level of theory (with ZPE included) the barriers are 6.8 (^{5}**TS1**) and 6.2 (^{5}**TS3**) kcal mol^{-1}, whereas with the LACV3P+* basis set (with ZPE at the LACVP level) barriers of 5.4 (^{5}**TS1**) and 5.9 (^{5}**TS3**) kcal mol^{-1} are obtained. These barriers are of the same order of magnitude as the gas-phase calculations described above, and

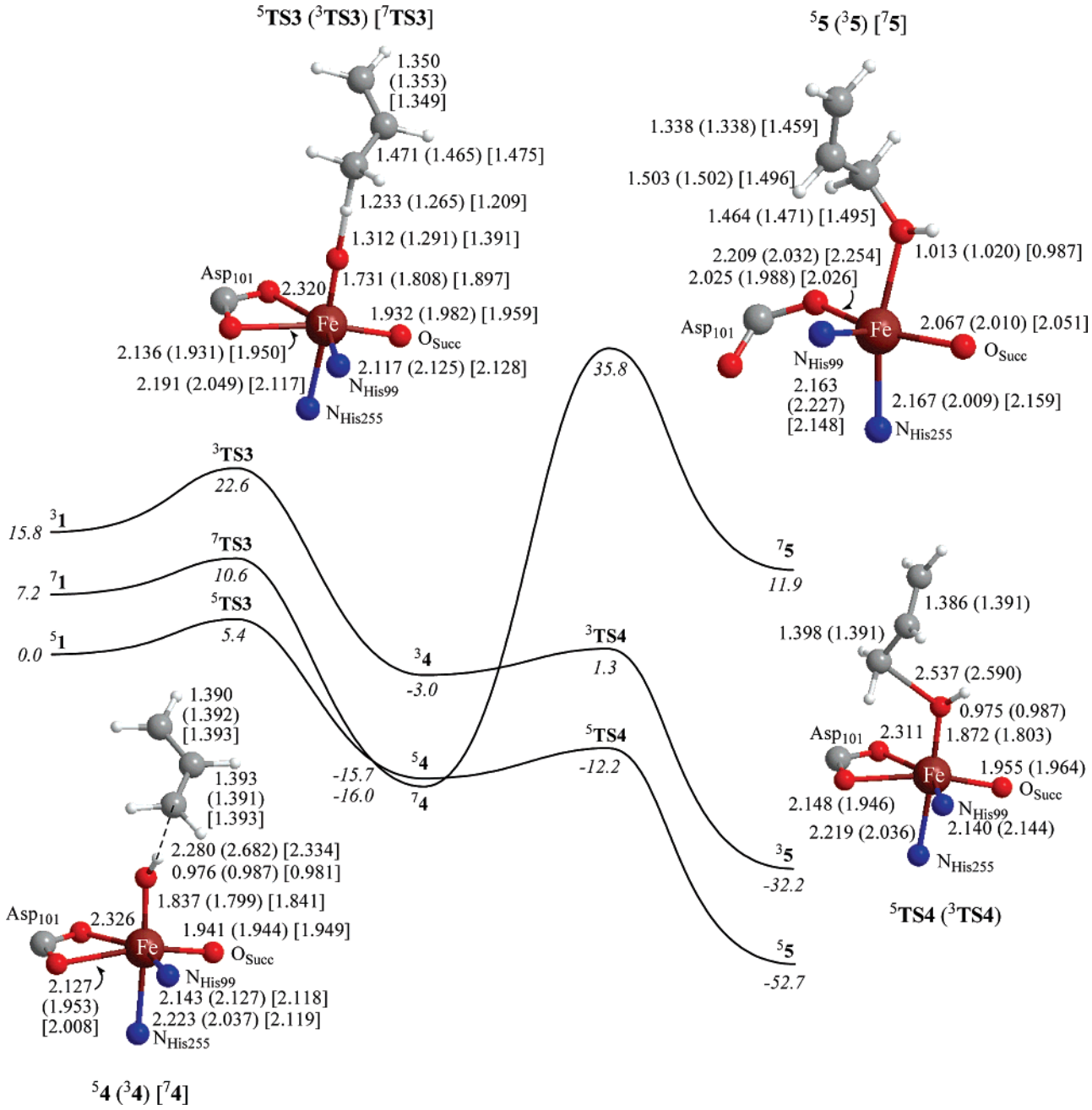

Figure 4. Reaction profile of the hydroxylation of propene by ^{3,5,7}**1** (αKGD) as obtained from UB3LYP/LACVP optimizations in Jaguar. All energies (in kcal mol^{-1}) are at the LACV3P+* level of theory with ZPE corrections included. Also shown are extracts of the optimized geometries along the pathway with bond lengths in Å.

therefore hydrogen bonded water molecules have limited effect on the relative energies of the barriers. This is not surprising since the imidazole groups do not participate in the electron-transfer processes which may influence these reaction barriers.

Finally, we estimated the kinetic isotope effect (KIE) using the Eyring (KIE_E) and Wigner (KIE_W) models for ^{5}**TS1** and ^{5}**TS3** (see Table 1). The largest KIE is obtained for ^{5}**TS3** for the fully deuterated propene and is 6.08 (KIE_E) and 7.55 (KIE_W). These values are significantly lower than the ones obtained experimentally for taurine vs taurine-d_2 for which a $k_H/k_D = 37$ was measured.[39] This is presumably, since we calculated a different substrate (propene vs taurine), so that a full QM/MM study on taurine hydroxylation by αKGD Cpd I will be required. It may very well be that the electrostatic interactions within the active pocket influence the taurine hydroxylation process whereby the deuterium substituted reaction is destabilized. The KIE values obtained here are also significantly lower than the ones obtained for a P450 Cpd I model in a reaction with propene where values of $KIE_W = 10.5$ and 7.7 for the quartet and doublet spin states were obtained, respectively.[23b] Surprisingly, the epoxidation mechanism has an inverse isotope effect of 0.85 when the terminal two hydrogen atoms on the double bond are replaced by deuterium atoms. Thus, although the epoxidation mechanism involves breaking of the C=C double bond and formation of a C−O bond, the hydrogen atoms on the terminal carbon atoms are not innocent spectators but contribute to the

(39) Price, J. C.; Barr, E. W.; Glass, T. E.; Krebs, C.; Bollinger, Jr.; J. M. *J. Am. Chem. Soc.* **2003**, *125*, 13008−13009.

Table 1. Kinetic Isotope Effects (KIE) as Calculated with the Eyring (KIE_E) and Wigner (KIE_W) Models for the Substitution of One or More Hydrogen Atoms in Propene by Deuterium Atoms and the Free Energy of Activation for Propene and Propene-d_6[a,b]

	^{5}TS1		^{5}TS3	
	KIE_E	KIE_W	KIE_E	KIE_W
propene-h_6/propene-$d^{\alpha}{}_1$	1.06	1.06	5.55	6.74
propene-h_6/propene-$d^{\beta\gamma}{}_2$	0.98	0.98	1.09	1.12
propene-h_6/propene-$d^{\delta}{}_1$	1.01	1.01	0.97	0.97
propene-h_6/propene-$d^{\epsilon}{}_2$	0.85	0.85	1.01	1.01
propene-h_6/propene-d_6	0.89	0.89	6.08	7.55
$\Delta G^{\ddagger}$ (propene-h_6)	6.62		7.37	
$\Delta G^{\ddagger}$ (propene-d_6)	6.55		8.44	

[a] The atoms are defined as follows: O- - -H$^{\alpha}$- - -CH$^{\beta}$H$^{\gamma}$—CH$^{\delta}$=CH$^{\epsilon}{}_2$, the superscript after propene-*d* gives the hydrogen atoms replaced by deuterium atoms and the subscript the total number of substitutions. [b] Free energies are in kcal mol^{-1} and obtained at the LACV3P+* level of theory with ZPE and thermal corrections at LACVP level of theory.

energetics. The secondary isotope effect on ^{5}**TS3** is 1.09 and 1.12 when both hydrogen atoms are replaced by deuterium atoms. Hydrogen by deuterium substitution of all atoms of propene leads to an increase of the methyl hydroxylation barrier by more than 1 kcal mol^{-1} (Table 1), whereas the epoxidation barrier changes only marginally.

Discussion

In this paper, we presented results of DFT calculations on the competitive epoxidation and hydroxylation mechanisms by an αKGD catalyst. Generally, the reactions proceed in a stepwise manner with low barriers of 4.8 (**TS1**) or 5.4 (**TS3**) kcal mol^{-1}. By contrast, the propene epoxidation by HRP and P450 Cpd I models predicted much higher barriers (**TS1**) of 8.5 and 12.3 kcal mol^{-1}, respectively using the same methods and basis sets.[23,24] This means that αKGD Cpd I is a much more efficient oxygenation catalyst than heme-enzymes and should be able to hydroxylate strong C−H bonds. In the next sections, we will address the reasons that determine the fundamental factors that differentiate between the heme and non-heme oxo-iron catalysts.

Electronic Changes Along the Reaction Coordinate. The oxo-iron complex of αKGD enzymes has a quintet spin ground state with occupation: $\pi^*_{xz}{}^1\pi^*_{yz}{}^1\pi^{*1}_{x^2-y^2}\sigma^*_{xy}{}^1\sigma_{z^2}{}^{*0}$, whereas in the septet spin state the complete metal d-block plus a lone-pair on the oxo group (π_O) are singly occupied. In the triplet spin state four metal d-orbitals are singly occupied, three with α-spin (π^*_{xz}, π^*_{yz}, $\sigma^*_{z^2}$) and one with β-spin ($\pi_{x^2-y^2}$*). Attempts to create a triplet spin solution with $\pi^{*2}_{x^2-y^2}\pi^*_{xz}{}^1\pi^*_{yz}{}^1$ occupation failed and converted back to the open-shell situation of Figure 5. Because of lesser exchange stabilization in the triplet spin state than in the quintet spin state, ^{3}**1** is considerably higher in energy than ^{5}**1**.

Since, the epoxidation and hydroxylation mechanisms follow the same electron transfer mechanisms (Figure 5) along the reaction coordinate, for simplicity we will discuss only the epoxidation reaction. The initial C−O bond activation process in the epoxidation mechanism and the hydrogen abstraction in the hydroxylation mechanism involve the transfer of one electron from the substrate into the metal 3d-block. In both cases in the quintet spin state, an α-spin electron is transferred into the empty $\sigma^*_{z^2}$ orbital whereby in ^{5}**2** (and ^{5}**4**) a situation is created with the complete metal d-block singly occupied. In addition, there

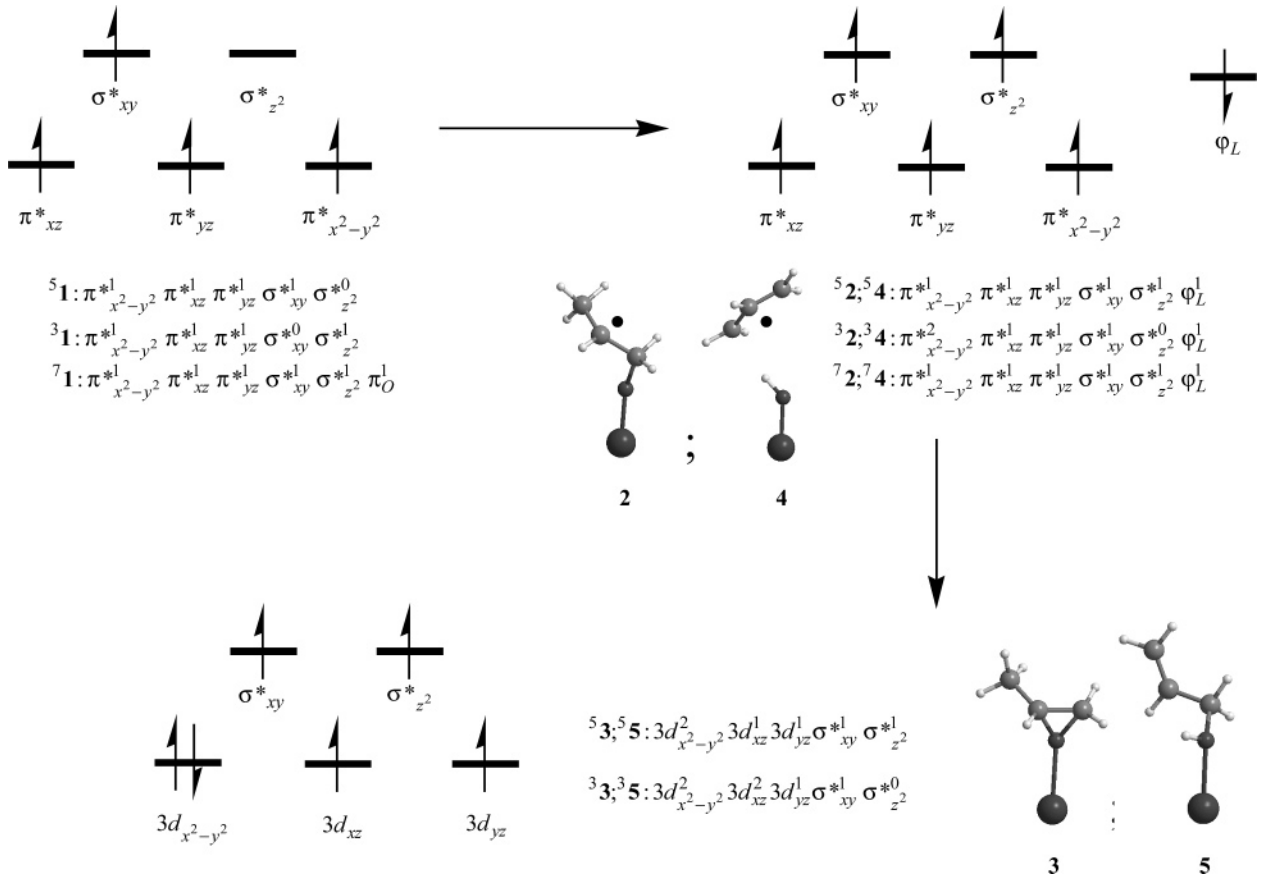

Figure 5. Orbital occupation of reactants, intermediates and products during the epoxidation and hydroxylation reactions.

is a radical center on the substrate with an electron with β-spin. Thus, in the quintet spin state the system gains radical character with six unpaired electrons including an exchange stabilized metal d-block, whereas in the triplet and septet spin states the number of singly occupied orbitals stays the same during the complete reaction process. In the septet spin state, the same intermediate state is reached as in the quintet spin state with the same orbital occupation, but with the substrate electron (φ_L) with an α-spin rather than β-spin. As a consequence of their similar electronic identity, the intermediate states (**2**, **4**) in the quintet and septet spin states are close in energy and chemical structure.

In the second step of the reaction (from **2** to **3** and from **4** to **5**) a second electron is transferred from the substrate to the metal, namely in the triplet and quintet spin states the β-spin (φ_L) electron moves into a 3d-metal orbital which becomes doubly occupied. Thus, the metal changes its oxidation state from Fe^{IV} in the reactant complex via Fe^{III} in the intermediates to Fe^{II} in the product complexes. In the product complex, the oxygen atom has been transferred to the substrate and does not give molecular orbital overlap with the metal anymore whereby the π^*_{xz}, π^*_{yz} and $\pi^*_{x^2-y^2}$ orbitals of Cpd I are essentially converted into atomic 3d orbitals in the product complexes ($3d_{xz}$, $3d_{yz}$, and $3d_{x^2-y^2}$). One of those ($3d_{x^2-y^2}$) is doubly occupied in the quintet spin state, while in the triplet spin state also the $3d_{xz}$ is doubly occupied. In the septet spin state the complete metal 3d block is singly occupied plus a lone-pair orbital on the oxo group. The latter orbital is filled in the first step of the reaction whereby a radical intermediate (^{7}**2**, ^{7}**4**) is created. However, due to the absence of accessible low-lying virtual orbitals to accept the last electron, in the septet spin state the reaction from ^{7}**2** or ^{7}**4** leads either to dissociation into $CH_2O + CH_3CH\bullet\bullet$ or to biradical hydroxylation products. Therefore, the septet spin state can only compete with the quintet spin state in the first part of the reaction pathways, but due to the lack of a second oxidizing equivalent the reaction stops there. Thus, to convert ^{7}**2** and ^{7}**4** into product complexes, a spin state crossing to a lower spin state is necessary. The triplet spin state is high lying during the complete reaction process, and will not play a major contribution in catalysis. In conclusion, αKGD will react via single-state reactivity (SSR) on a dominant quintet spin state surface.

The electronic ground state of αKGD Cpd I and the subsequent electron-transfer processes during the oxygenation process is in sharp contrast to the one obtained for heme-enzymes. Although, both αKGD and P450 Cpd I have the metal in the same oxidation state (Fe^{IV}), there are some essential differences in the properties of the catalyst. In particular, in heme-systems the t_{2g} set of π^* orbitals splits in a one-below-two subset (δ, π^*).[7c] Two of these orbitals (π^*_{xz}, π^*_{yz}) are essentially the same as the ones in αKGD (Figure 1), but the third one ($\delta_{x^2-y^2}$) is a nonbonding orbital whereas the corresponding $\pi^*_{x^2-y^2}$ in αKGD Cpd I is an antibonding orbital. Therefore, αKGD Cpd I has four electrons in antibonding orbitals, while P450 Cpd I with orbital occupation $\delta^2\,\pi^*_{xz}{}^1\,\pi^*_{yz}{}^1\,a_{2u}{}^1$ has two electrons in a nonbonding orbital (δ) and two in antibonding orbitals. Consequently, αKGD Cpd I will be much more reactive than P450 Cpd I and indeed our reactivity studies confirm this. Because of double occupation of this low-lying δ orbital in heme-enzymes the overall spin state of the system is reduced. In addition, heme-enzymes have an extra oxidizing equivalent on the heme, which contains a radical due to single occupation of the a_{2u} orbital. Thus, during the reaction mechanism one electron is shuttled away from the reaction center into the heme-ligand, which is not possible in non-heme systems like αKGD. During the reaction process, in P450 enzymes the metal is reduced from oxidation state Fe^{IV} to Fe^{III}, whereas in αKGD the metal is reduced by two units to Fe^{II}.

Other DFT studies on synthetic non-heme oxo-iron compounds[21b] used a pentadentate ligand (N4Py), which has four nitrogen atoms in the *xy*-plane of symmetry similarly to heme-enzymes. As a result, non-heme oxo-iron compounds with an N4Py ligand have similar molecular orbitals as heme-enzymes, namely a doubly occupied nonbonding $\delta_{x^2-y^2}$ orbital rather than a $\pi^*_{x^2-y^2}$ antibonding orbital. These systems, therefore, will behave similarly to heme-type oxo-iron systems with two-state reactivity (TSR) patterns on competing spin state surfaces and behave differently to the TauD models as described here.

Differences in the initial electron-transfer processes between P450 and αKGD result in geometric differences of the transition states (Figure 6). Thus, in αKGD Cpd I an electron is transferred from the double bond of propene into the empty $\sigma^*_z{}^2$ orbital, which is antibonding along the Fe−O bond. Hence, in **TS1** the double bond is almost linearly aligned with the oxo-iron group as can be seen from the geometries in Figure 6, whereby the Fe−O−C angle in ^{5}**TS1** is 154.5°. Similarly, the hydrogen abstraction reaction due to aligning of molecular orbitals results in an Fe−O−H angle in ^{5}**TS3** of 175.9°. By contrast, in heme-enzymes such as P450 the electron is transferred into a singly occupied π^*_{FeO} orbital so that the double bond will approach from the side to obtain maximum overlap. Therefore, differences in orbital overlap between the reactants results in variations in transition state geometries. Moreover, it will have consequences on the shape and size of the substrate bound pocket in the enzyme but these studies need to await a full QM/MM approach.

Competitive Epoxidation and Hydroxylation. The hydroxylation and epoxidation mechanisms of propene activation by ^{5}Cpd I (αKGD) are summarized in Figure 7. Both reaction mechanisms are stepwise via an intermediate radical complex leading to products, although the first step is rate determining. In the gas-phase there is a small preference for epoxidation over hydroxylation by 0.6 kcal mol^{-1}. The two surfaces are close in energy during the first step of the reaction but in the product complexes they bifurcate due to differences in stability of the epoxide vs propenol products. This energy difference of 13.2 kcal mol^{-1} is identical to the one obtained between the product complexes in the doublet spin state of a P450 model Cpd I.[23b]

On both surfaces the intermediates (^{5}**2**, ^{5}**4**) are separated by a small barrier from products. This means that the intermediate complexes will have a finite lifetime during which rearrangements can occur. For instance, an internal rotation along the CH−CH_2 bond in ^{5}**2** may lead to cis/trans scrambling or a hydrogen atom transfer can produce aldehyde product complexes.[40] The rebound barrier (**TS4**) is similar to the one obtained for P450 Cpd I, but the ring-closure barrier (**TS2**) is somewhat larger.[23]

Small perturbations such as a dielectric constant change the ordering of ^{5}**TS1** and ^{5}**TS3** so that in $\epsilon = 5.7$ and $\epsilon = 10.65$ the hydroxylation pathway is favored. By contrast, substitution

(40) Kumar, D.; de Visser, S. P.; Shaik, S. *Chem.—Eur. J.* **2005**, *11*, 2825−2835.

Table 2. Comparisons of the Electronic Properties of Various Oxo-Iron Complexes as Calculated by DFT

	ligand-type	spin state	orbital occupation[a]	oxidation state	ref
αKGD	non-heme	quintet	$\pi^{*1}_{x^2-y^2}\pi^{*}_{xz}{}^{1}\pi^{*}_{yz}{}^{1}\sigma^{*}_{xy}{}^{1}$	Fe(IV)	this work
P450	heme	quartet/doublet	$\delta^{2}_{x^2-y^2}\pi^{*}_{xz}{}^{1}\pi^{*}_{yz}{}^{1}a_{2u}{}^{1}$	Fe(IV)	23
HRP	heme	quartet/doublet	$\delta^{2}_{x^2-y^2}\pi^{*}_{xz}{}^{1}\pi^{*}_{yz}{}^{1}a_{2u}{}^{1}$	Fe(IV)	24
C*c*P	heme	quartet/doublet	$\delta^{2}_{x^2-y^2}\pi^{*}_{xz}{}^{1}\pi^{*}_{yz}{}^{1}\pi_{Trp}{}^{1}$	Fe(IV)	26
CpdI−Cl	heme	quartet/doublet	$\delta^{2}_{x^2-y^2}\pi^{*}_{xz}{}^{1}\pi^{*}_{yz}{}^{1}a_{2u}{}^{1}$	Fe(IV)	41

[a] The αKGD orbitals are labeled as in Figure 1. The radical on the heme is a_{2u} and the radical on tryptophan in C*c*P is π_{Trp}.

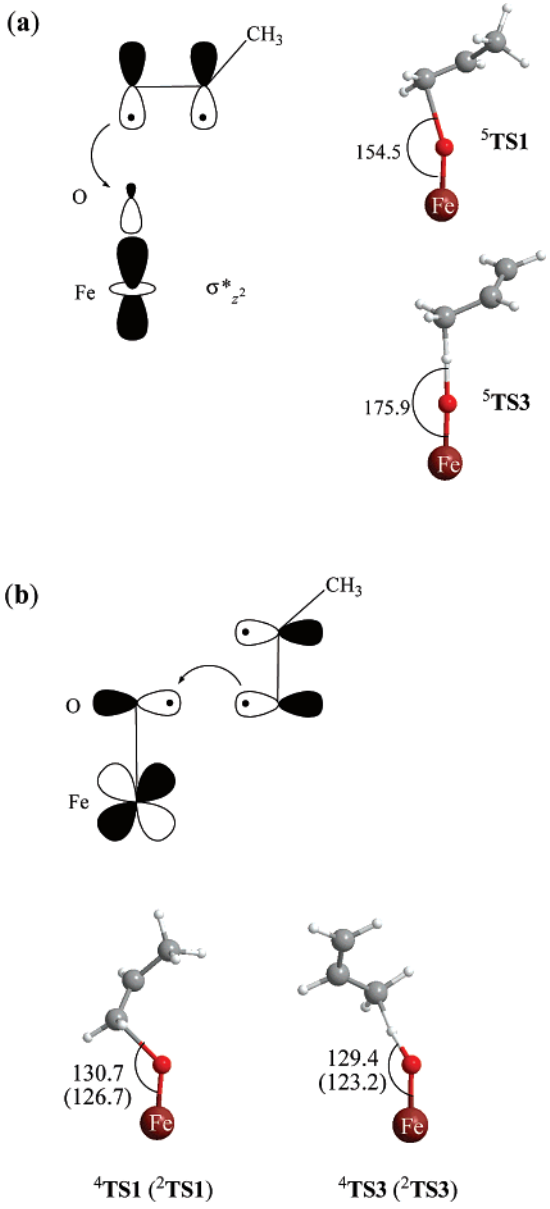

Figure 6. Electron-transfer processes in (a) αKGD and (b) P450. Also shown are highlights of the epoxidation (**TS1**) and hydroxylation (**TS3**) transition states from (a) this work and (b) ref 23.

of hydrogen atoms of propene by deuterium atoms leads to an increase of the hydrogen abstraction barrier since a C−D bond is stronger than a C−H bond, thereby disfavoring the hydroxylation pathway. Therefore, subtle changes in the local environment of the catalyst as well as isotopic substitutions can influence the reaction barriers and hence the product distributions.

Comparison of Cpd I of Non-Heme vs Heme Systems. Oxo-iron complexes appear in many different enzymes such as

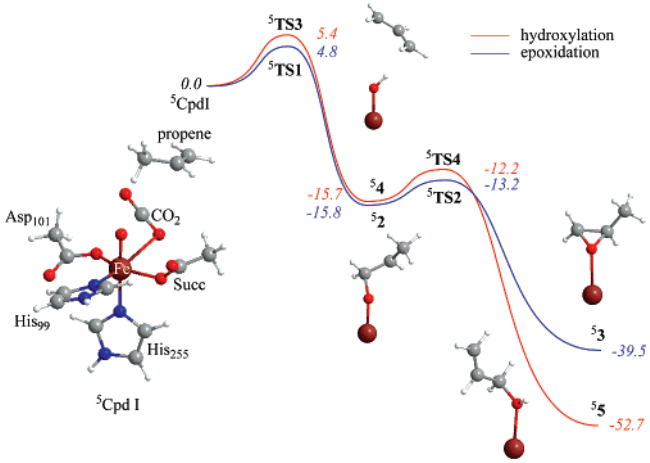

Figure 7. Potential energy surfaces for the propene epoxidation and hydroxylation mechanisms by ^{5}Cpd I of αKGD. All energies are relative to reactant complex in kcal mol^{-1} and taken from the LACV3P+* energies with ZPE corrections at LACVP level of theory.

Table 3. Comparisons of the Reactivity Patterns of Oxo-iron Complexes with Propene as Calculated with DFT[a]

	reactivity pattern[b]	**TS1**[c]	**TS3**[c]	ref
αKGD	SSR	4.8	5.4	this work
P450	TSR	12.8 (12.3)	14.0 (13.0)	23
HRP	TSR	9.7 (8.5)	10.9 (9.7)	24
CpdI−Cl	TSR	12.7 (11.7)	14.8 (12.9)	41

[a] All energies are in kcal mol^{-1} and obtained at UB3LYP/LACV3P+* level with ZPE corrections at LACVP level of theory. [b] SSR = single-state reactivity and TSR = two-state reactivity. [c] Heme systems obtained at the quartet (doublet) spin states.

P450, HRP, and αKGD. However, in all systems, the oxo-iron unit is in a different environment which influences the catalytic properties of the system. Thus, the P450s contain a thiolate ligand from a cysteinate residue which entices a push-effect, whereas the imidazole group of the axial bound histidine pulls electrons in HRP.[2−5] Both, HRP and P450 are heme-enzymes but have different uses in biosystems, namely HRP functions as an electron sink and reduces hydrogen peroxide to water, whereas the P450s catalyze monoxygenation reactions. Five-coordinated oxo-iron complexes as appear in αKGD enzymes also catalyze monoxygenation reactions. Tables 2 and 3 summarize the different properties of αKGD, P450, and HRP with respect to monoxygenation of propene as revealed by DFT calculations on model complexes.[22−25,41] In Table 2, CpdI−Cl represents a biomimetic oxo-iron porphyrin model with a chloride axial ligand.

Generally, heme-type enzymes contain two close-lying spin states as electronic ground state, i.e., doublet and quartet spin, with the same orbital occupation. As a result, the substrate monoxygenation by heme-complexes takes place on competing

(41) de Visser, S. P. *J. Biol. Inorg. Chem.* **2006**, *11*, 168−178.

doublet and quartet spin surfaces, which is termed two-state reactivity (TSR).[42] By contrast, non-heme five-coordinated oxo-iron complexes, such as αKGD, react on a dominant quintet spin surface via single-state reactivity (SSR). Heme-enzymes not always react via TSR with substrates, since, for instance, benzene hydroxylation was shown to appear on a dominant doublet spin state surface while sulfoxidation is favorable in the quartet spin state.[43] In P450 systems, it was shown that in some cases the reaction mechanisms are different on the two spin state surfaces so that they can masquerade as different oxidants.[43b] Moreover, it was shown that side reactions in epoxidation reactions leading to suicidal complexes or aldehyde complexes can only occur on the quartet spin surface and not on the doublet one and as a result the two spin state surfaces produce products with different distributions and rate constants.[40,44] This is not the case with αKGD oxo-iron complexes since they react via SSR, with in principle the quintet spin state as the sole oxidant.

The reactivity patterns of the various enzyme models show some similarities, such as stepwise reaction mechanisms via radical intermediates. In fact, in the case of propene monoxygenation in all enzyme models studied the epoxidation is slightly (0.6−1.2 kcal mol^{-1}) below the hydroxylation mechanism. Moreover, calculations in a dielectric constant showed that the hydroxylation mechanisms are stabilized.

Mayer[45] discovered that for oxo-metal complexes the hydrogen abstraction barrier, or the rate constant of C−H hydroxylation of an alkane (Alk-H), is linearly correlated to the energy to break the C−H bond in the substrate (BDE_{C-H}) as well as to the energy of the newly formed O−H bond (BDE_{O-H}), eqs 4 and 5. A similar correlation for non-heme oxo-iron complexes was proposed by Kaizer et al. for pentadentate complexes.[46] It was shown that C−H bonds of alkanes with a strength of up to 99.3 kcal mol^{-1} were hydroxylated. Thus, the sum of eqs 4 and 5 gives the exothermicity of the hydrogen abstraction step from reactants leading to intermediates (**4**) and is correlated to the bond dissociation energies of the C−H and O−H bonds (eq 6).[47]

$$\text{Alk-H} \rightarrow \text{Alk}\bullet + \text{H}\bullet + BDE_{C-H} \quad (4)$$

$$\text{FeO}-\text{H} \rightarrow \text{Fe}{=}\text{O} + \text{H}\bullet + BDE_{O-H} \quad (5)$$

$$\text{Fe}{=}\text{O} + \text{Alk-H} \rightarrow \text{FeO}-\text{H} + \text{Alk}\bullet \quad (6)$$

The enthalpy difference (ΔH_r) for eq 6 is

$$\Delta H_r \text{ (eq 6)} = BDE_{C-H} - BDE_{O-H} \quad (7)$$

In the past, we and others calculated the hydroxylation of propene by oxo-iron complexes mimicking the active sites of P450,[23] HRP,[24] a heme-model with chloride axial ligand (CpdI−Cl)[41] and a polyoxometalate (POM).[48] Using the BDE_{C-H} of propene from ref 47 we calculated the reaction exothermicity of eq 6 and used it to estimate BDE_{O-H} for these oxo-iron catalysts and the results are shown in Figure 8. In the case of POM, Shaik et al.[48] did not perform a frequency calculation for the intermediate species **4** but we estimated it from trends of previous work (see Supporting Information). As can be seen the heme-models give almost identical O−H bond dissociation energies of 88.7 kcal mol^{-1}. Surprisingly, also the POM gives a BDE of the same order of magnitude as the heme-enzymes, whereas the electronic structure is considerably different. Still, the largest BDE_{O-H} value obtained is for αKGD, which is almost 10 kcal mol^{-1} larger than the other catalysts.

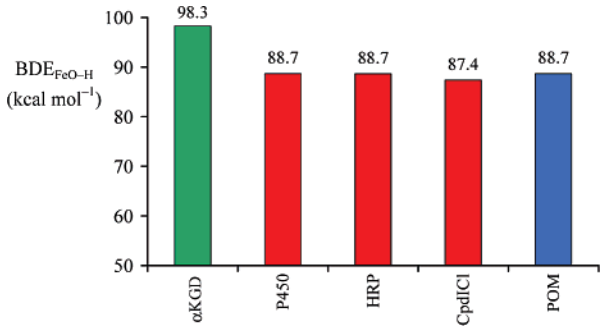

Figure 8. FeO−H bond dissociation energies (BDE_{O-H}) of several oxo-iron complexes as calculated with DFT UB3LYP/LACV3P+* with ZPE corrections at LACVP level of theory. Green is the non-heme TauD model, red are heme-enzyme models and blue a polyoxometalate (POM).

So why does αKGD Cpd I have a large BDE_{O-H} and how does it influence the reaction kinetics? To correlate the two consider in Figure 9 the Valence Bond electron-transfer mechanism for the hydrogen abstraction reaction from ^{5}**1** to ^{5}**4**. In the reactants there is a pair of electrons in the C−H bond, a doubly occupied lone-pair on oxygen along the Fe−O axis (π_O) and four electrons in the metal 3d system ($\pi^*_{xz}{}^1\pi^*_{yz}{}^1\pi^*{}^1_{x^2-y^2}$-$\sigma^*_{xy}{}^1\sigma^*{}^0_{z^2}$) and ^{5}**1** has total wave function $^5\Psi_R$. In the intermediate (^{5}**4**), the wave function ($^5\Psi_I$) is quite different namely there is a radical center on a carbon atom of the substrate, two electrons in the O−H bond and the metal 3d system is fully occupied with five electrons. The $^5\Psi_R$ and $^5\Psi_I$ wave functions cross in the transition state (^{5}**TS3**), which energetically is a fraction (f) of the vertical excitation energy (G) at the reactant geometry.[49] From the orbital occupations in Figure 9, it follows that the excitation energy (G) between the two states is equal to the singlet−triplet energy gap of the C−H bond plus the excitation energy of an electron from π_O to $\sigma^*_z{}^2$. As shown before,[49] the singlet−triplet energy gap for the C−H bond is proportional to BDE_{C-H}. Therefore, the height of the barrier ^{5}**TS3** is also proportional to BDE_{C-H} and because of eq 7 to BDE_{O-H} as well. A similar correlation was recently shown for oxo-iron heme-enzymes.[47] This shows that αKGD catalysts are extremely powerful catalysts of oxygenation reactions and should be able to catalyze hydroxylation reactions of substrates with strong C−H bonds. In fact, the actual BDE_{O-H} of αKGD will be even higher than 98.3 kcal mol^{-1} since the energy difference taken for this datum is between a reactant complex

(42) Shaik, S.; de Visser, S. P.; Ogliaro, F.; Schwarz, H.; Schröder, D. *Curr. Opin. Chem. Biol.* **2002**, *6*, 556−567.
(43) (a) de Visser, S. P.; Shaik, S. *J. Am. Chem. Soc.* **2003**, *125*, 7413−7424. (b) Sharma, P. K.; de Visser, S. P.; Shaik, S. *J. Am. Chem. Soc.* **2003**, *125*, 8698−8699. (c) Kumar, D.; de Visser, S. P.; Sharma, P. K.; Cohen, S.; Shaik, S. *J. Am. Chem. Soc.* **2004**, *126*, 1907−1920. (d) de Visser, S. P.; Kumar, D.; Shaik, S. *J. Inorg. Biochem.* **2004**, *98*, 1183−1193. (e) Kumar, D.; de Visser, S. P.; Sharma, P. K.; Hirao, H.; Shaik, S. *Biochemistry* **2005**, *44*, 8148−8158.
(44) de Visser, S. P.; Ogliaro, F.; Shaik, S. *Angew. Chem., Int. Ed.* **2001**, *40*, 2871−2874.
(45) Mayer, J. M. *Acc. Chem. Res.* **1998**, *31*, 441−450.
(46) Kaizer, J.; Klinker, E. J.; Oh, N. Y.; Rohde, J.-U.; Song, W. J.; Stubna, A.; Kim, J.; Münck, E.; Nam, W.; Que Jr., L. W. *J. Am. Chem. Soc.* **2004**, *126*, 472−473.
(47) de Visser, S. P.; Kumar, D.; Cohen, S.; Shacham, R.; Shaik, S. *J. Am. Chem. Soc.* **2004**, *126*, 8362−8363.
(48) Kumar, D.; Derat, E.; Khenkin, A. M.; Neumann, R.; Shaik, S. *J. Am. Chem. Soc.* **2005**, *127*, 17712−17718.
(49) Shaik, S.; Shurki, A. *Angew. Chem., Int. Ed. Engl.* **1999**, *38*, 586−625.

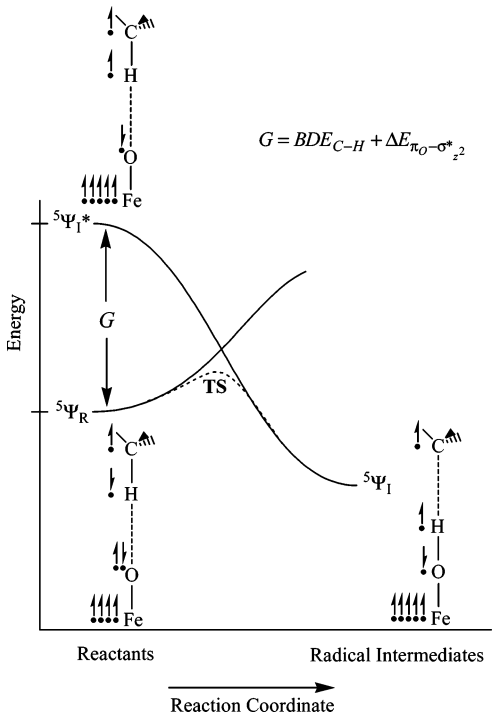

Figure 9. Valence bond curve crossing diagram for the hydrogen abstraction step from ^{5}**1** to ^{5}**4** in TauD. The electrons next to iron represent the 3d orbitals as depicted in Figure 1 and the ones next to oxygen are electrons occupying the π_O orbital along the Fe−O bond.

and the intermediate complex, whereas in all other situations the energies are with respect to isolated reactants. This will increase the exothermicity of the intermediate complex by a couple of kcal mol^{-1} more. Nevertheless, the trend in Figure 8 clearly shows that the newly formed O−H bond in five-coordinated oxo-iron complexes as appear in αKGD enzymes are much stronger than corresponding systems in a heme environment. As a consequence, the reaction barriers for hydroxylation and epoxidation mechanisms of substrates are considerably lowered as compared to heme-enzymes, which we indeed observed here. Therefore, αKGD is a very potent catalyst which should be able to hydroxylate strong C−H bonds, while the heme-enzymes are more subtle hydroxylating agents.

Conclusions

Density functional calculations on the reactivity patterns of oxo-iron complexes versus propene are reported. Models of αKGD and P450 are studied, which differ in the number of ligands around iron and are five-coordinated and six-coordinated complexes, respectively. Our calculations show that six-coordination of the metal changes an antibonding (π*) orbital into a nonbonding orbital, as a result the five-coordinate reactant is in a quintet spin ground state, whereas the six-coordinate systems have lower spin states. Moreover, oxo-iron heme systems have a second oxidizing equivalent on the heme, which gives the system close-lying quartet and doublet spin states. As a result, the metal is reduced by only one unit in heme-enzymes, while in five-coordinated non-heme systems the metal is reduced from oxidation state Fe^{IV} to Fe^{II} during the reaction process. The five-coordinated non-heme oxo-iron catalysts are potent and aggressive oxygenation catalysts with much lower reaction barriers than heme-enzymes because (i) the newly formed FeO−H bond is much stronger, (ii) the system gains radical character in the initial and rate-determining reaction step, and (iii) the metal d-block is exchange stabilized.

Acknowledgment. The National Service of Computational Chemistry Software (NSCCS) is acknowledged for providing CPU time.

Supporting Information Available: 24 tables and 4 figures with data are available plus full ref 31. This material is available free of charge via the Internet at http://pubs.acs.org.

JA061581G